

E15-2008-118

J. Adam^{1,2,*}, K. Katovský^{1,3}, M. Majerle², M. I. Krivopustov¹,
V. Kumar⁴, Manish Sharma⁴, Chitra Bhatia⁴, A. A. Solnyshkin¹,
V. M. Tsoupko-Sitnikov¹

TRANSMUTATION OF Th AND U WITH NEUTRONS
PRODUCED IN Pb TARGET AND U-BLANKET SYSTEM
BY RELATIVISTIC DEUTERONS

Submitted to «Nuclear Instruments and Methods A»

¹ Joint Institute for Nuclear Research, Dubna, Russia

² Czech Academy of Sciences, Nuclear Physics Institute, Řež,
Czech Republic

³ Department of Nuclear Reactors, Czech Technical University in Prague,
Czech Republic

⁴ HENP Laboratory, Physics Department, University of Rajasthan, Jaipur,
India

* E-mail: iadam@jinr.ru

Адам И. и др.

E15-2008-118

Трансмутация Th и U нейтронами, образующимися в результате взаимодействия релятивистских дейтронов в системе Pb-мишень – U-бланкет

Свинцовая мишень, окруженная подкритическим урановым бланкетом (система «Энергия плюс трансмутация»), облучалась дейтронами с энергией 1,6 ГэВ на ускорителе нуклотрон Лаборатории высоких энергий ОИЯИ (Дубна). Нейтроны, возникающие за счет реакции скалывания в свинцовой мишени, взаимодействовали с подкритическим бланкетом. Образцы урана и тория, расположенные на поверхности бланкета, облучались нейтронным полем. Выход продуктов реакций («остаточные ядра») определялся методами гамма-спектрометрии и использовался для расчета трансмутационной способности установки. Экспериментальные результаты сравнивались с расчетами Монте-Карло по программе MCNPX 2.6.c и с результатами эксперимента TARC.

Работа выполнена в Лаборатории ядерных проблем им. В. П. Дзелепова ОИЯИ.

Препринт Объединенного института ядерных исследований. Дубна, 2008

Adam J. et al.

E15-2008-118

Transmutation of Th and U with Neutrons Produced in Pb Target and U-Blanket System by Relativistic Deuterons

Lead target and uranium blanket setup called «Energy plus Transmutation» was irradiated by 1.6 GeV deuteron beam from the Nuclotron accelerator at the Laboratory of High Energies of Joint Institute for Nuclear Research (Dubna). Neutrons generated by spallation reactions of deuterons with lead target interact with subcritical uranium blanket. In the neutron field outside the blanket radioactive uranium and thorium samples were irradiated. Reaction rate of some residual nuclei determined using the method of gamma-spectrometry in the experiment is used to calculate the transmutation power of the setup. Experimental results are compared with the Monte Carlo calculation performed by the MCNPX 2.6.C code and with some results of the TARC experiment.

The investigation has been performed at the Dzhelepov Laboratory of Nuclear Problems, JINR.

Preprint of the Joint Institute for Nuclear Research. Dubna, 2008

INTRODUCTION

Accelerator Driven Subcritical Systems (ADS) are the projects which not only give new ideas related to the end products of a fuel cycle but are very useful in developing the field of high energy neutrons. Such systems can be used to incinerate long-lived fission products and minor actinides produced by conventional fission reactors. Specially, ADS may prove to be useful to incinerate large amount of plutonium accumulated from nuclear weapons and because of the availability of high energy neutrons, (n, xn) reactions may also add in the process of incineration along with the fission process. Inside such a system, high neutron flux is generated from the thick heavy metal target by the spallation reaction, and transmutation of selected isotopes may take place in the subcritical blanket. Reactions like $^{232}\text{Th}(n, 2n)$, $^{232}\text{Th}(n, 3n)$ and even higher order (n, xn) reactions contribute towards the neutron multiplication for the proposed ^{232}Th fuel on one hand and, on the other hand, reactions like (n, γ) with $^{\text{nat}}\text{U}$ and ^{232}Th are important due to the production of fissionable nuclei like ^{239}Pu and ^{233}U , respectively. In this situation, under the unusual mixed fields of low to very high energy neutron physics study of the (n, γ) , (n, f) and (n, xn) reactions from the point of transmutation and in turn transmutation power of the ADS becomes important. Inspired from the wide possibilities of incineration of the nuclear waste not only in Europe programs like PDS-XADC are started but many nuclear countries (USA, Russia, France, Japan, and India) laid down their road maps of ADS with the objectives of incineration of nuclear waste, energy production from the waste and to make use of fertile fuel like a thorium [1–3] for energy production. In this direction, Transmutation by Adiabatic Resonance Crossing (TARC) experiment [4] is one of the most leading step forward. Similarly, «Energy plus Transmutation» facility at JINR, Dubna is another setup developed during the last one decade at a rather small scale for the physics studies of ADS. In this paper, a method of estimation of transmutation power based on the experimental study of reaction rates of the residual nuclei has been presented and a comparison of calculated data with the results of our experiment using the «Energy plus Transmutation» setup has been made along with some of the experimental results of the TARC experiment.

1. EXPERIMENTAL SETUP

The «Energy plus Transmutation» setup, shown in Fig. 1, is a system of lead target and uranium blanket [5]. In the total length of 480 mm of the four sections, length of lead target is 456 mm. The diameter of lead is 84 mm and its total mass is 28.7 kg. The blanket contains four sections (see Fig. 1). Each

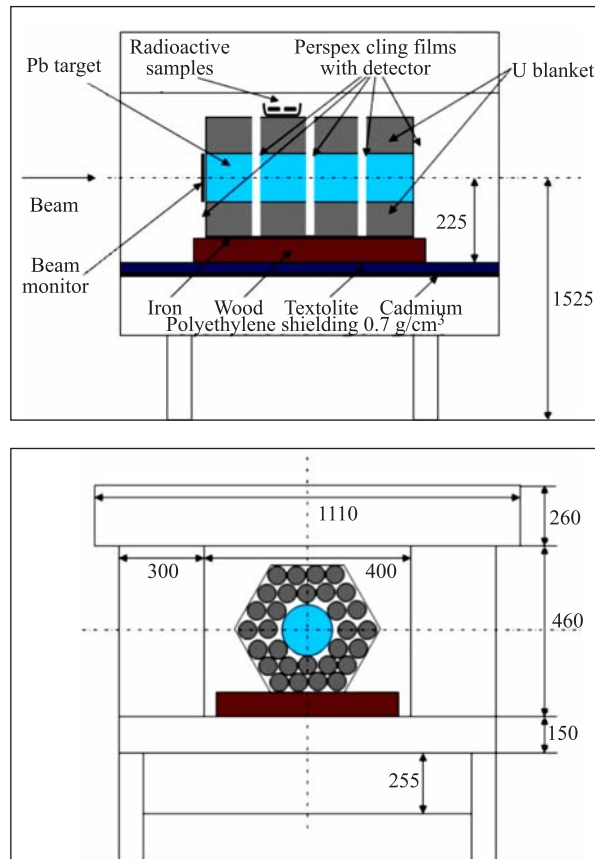


Fig. 1. Simplified front and side view of design of the «Energy plus Transmutation» setup inside its shielding as used in the experiment

section contains 30 uranium rods and each rod is wrapped in Al shell. Total mass of each section is 51.6 kg of natural uranium, so the whole blanket mass is 206.4 kg. Between each two sections there are gaps of 8 mm width in which



Fig. 2. Top view of the «Energy plus Transmutation» setup with radioactive samples. Beam enters from the left side. The circular samples are assumed to occupy volume of dimensions $36 \times 36 \times 1.5 \text{ mm}^3$ for the sake of simulation by MCNPX

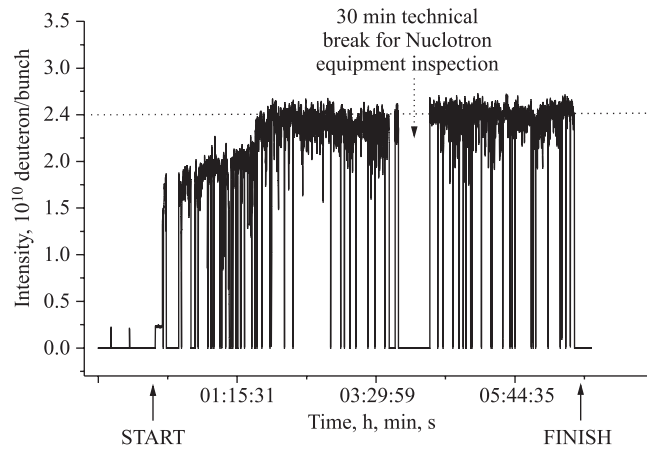


Fig. 3. Intensity profile of the 1.6 GeV deuteron beam (as received by the Nuclotron staff) used for irradiation of the Pb target

experimental instruments and detectors may be inserted. The entering side of the beam is covered with the beam monitor of aluminum and other activation or

Table 1. Deuteron beam ($E_d = 1.6$ GeV) profile

i -number of Al foils	$D(i)-D(i-1)$, cm	Weight, mg	$Q(^{24}\text{Na})$, s^{-1}	Activity, Bq	N_d^* , s^{-1}	N_D/S , cm^{-2}	Flux, $N_d \text{ cm}^{-2} \text{ s}^{-1}$
1	2.1 – 0.0	24	196(6)	60.41	8.18E+07	5.66E+11	2.36E+7
2	8.0 – 2.1	318	1735(42)	534.6	7.24E+08	3.70E+11	1.55E+7
3	12.0 – 8.0	428	496(13)	152.5	2.07E+08	7.89E+10	0.33E+7
4	16.0 – 12.0	598	28(2)	8.6	1.17E+07	3.18E+9	1.33E+5

* See Eqs. (1) and (2).

solid-state nuclear track detectors (SSNTD). On the top of the second section of blanket $^{\text{nat}}\text{U}$ and ^{232}Th samples, a set of other radioactive samples (^{129}I , ^{238}Pu , ^{239}Pu , and ^{237}Np), and threshold detectors have been placed as shown in Fig. 2. Uranium and thorium samples were irradiated in the form of sandwiches of three identical foils (Th-Th-Th and U-U-U). This arrangement has an advantage of accounting for the recoil residual nuclei produced in the middle foil. Diameter of these foils is 15 mm and weight of middle U foil is 172 mg and that of the middle Th foil is 93.2 mg. The «Energy plus Transmutation» setup was irradiated by the deuteron beam of 1.6 GeV at the Nuclotron accelerator in Dubna. The irradiation was started at 0:03 am on 18 December 2006 and lasted 399 minutes. The intensity profile of beam during the time of experiment is shown in Fig. 3 and in Table 1. Integral number of deuterons N_D hitting the Pb target is $1.93(25) \cdot 10^{13}$.

2. BEAM INTENSITY

The total number of deuterons hitting the lead target is obtained from thin aluminum monitors which are subsequently processed by the standard gamma-spectrometry method. The Al monitor contains a stack of three thin aluminum foils of $6.6975 \text{ mg}\cdot\text{cm}^{-2}$ thickness each. Due to recoil product nuclei the central foil was used for measurements. The stack of Al foils was mounted approximately 60 cm before the Pb target in order to avoid activation from backscattered particles and neutrons [6]. For monitoring purpose the reaction $^{27}\text{Al}(d, 3p2n)^{24}\text{Na}$ was used. The value of production cross sections for ^{24}Na at high energies are available for 2.33 GeV [7], 6 GeV and 7.30 GeV deuteron energies [8] and they are $15.25 \pm 1.5 \text{ mb}$, $14.1 \pm 1.3 \text{ mb}$ and $14.7 \pm 1.2 \text{ mb}$, respectively. At relativistic energies two nucleons in deuteron behave approximately as two separate entities [9]. Thus, the ratio of experimental values of $\sigma(^{27}\text{Al}(1.165 \text{ GeV}/A d, 3p2n)^{24}\text{Na}) / \sigma(^{27}\text{Al}(1.165 \text{ GeV } p, 3pn)^{24}\text{Na})$ is 1.495 [10]. In the same way, for 0.8 GeV/A deuteron energy using measured value for proton cross section to be $\sigma(^{27}\text{Al}(0.81 \text{ GeV } p, 3pn)^{24}\text{Na}) = 10.07(20) \text{ mb}$ [11] we got $\sigma(^{27}\text{Al}(0.8 \text{ GeV}/A d, 3p2n)^{24}\text{Na})$ to be 16.03 mb. Practically, the Al foil was cut into 3 concentric

rings with external diameters of 80, 120, and 160 mm and a central disc with diameter of 21 mm. We measured these rings and the central disc in order to determine their activities for deducing the corresponding beam intensity and beam profile (see Table 1 and Fig. 4).

Table 2. Final value of deuteron beam intensity

<i>i</i> -number of foils	N_d , s^{-1}	err. (N_d), s^{-1}	N_d , integral	err. (N_d), integral	Fraction of the sum
1+2	8.06E+08	2.00E+07	1.93E+13	4.80E+11	78.7(2)%
3+4	2.18E+08	5.74E+07	5.23E+12	1.37E+11	21.3(6)%
Sum	10.24E+08	7.74E+07	2.45E+13	6.17E+11	100%

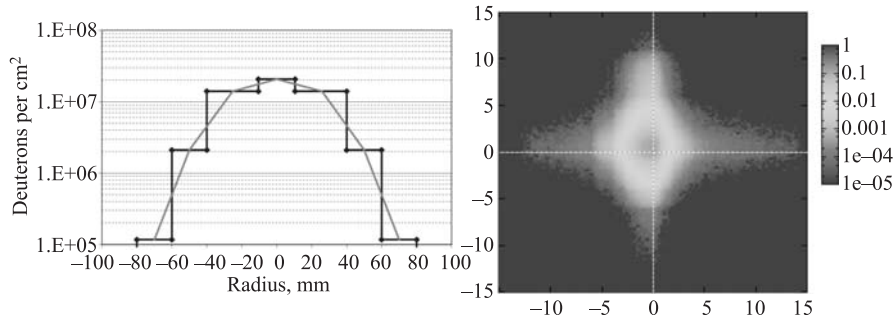


Fig. 4. Results of beam profile measurements. On the left panel the flux density is given in $N_d \text{ cm}^{-2} \cdot \text{s}^{-1}$ (see last column of Table 1). On the right panel is shown the «real beam» profile received by track detector [12]

The values of reaction rate $Q(^{24}\text{Na})$ given in Table 1 were corrected for fluctuations in the beam intensity ($\eta_B = 0.9865$) and for coincidence summing correction to be $\eta_C = 1.017$ for $E_\gamma = 1368 \text{ keV}$ and $\eta_C = 1.053$ for $E_\gamma = 2754 \text{ keV}$. The error in deuteron fluency corresponds to only statistical error in the calculation of $Q(^{24}\text{Na})$ value. This error must increase when one includes the systematic error for the extrapolated values of cross sections at lower energies because in literature there exists only a few experimental data. In the absence of the data at $0.8 \text{ GeV}/A$ deuteron energy we have assumed that the error cannot be more than 10%. The final values of integral beam intensity are given in Table 2.

Track detectors were used to determine the beam shape and from the data of track density versus space coordinate centroid and the width parameters of beam spot were determined [12]. Beam centroid is found to be at $X_c = -0.64 \text{ cm}$ and $Y_c = 0.39 \text{ cm}$ with respect to the axis of the «Energy plus Transmutation» setup

and FWHM, $X = 2.87$ cm and $Y = 1.92$ cm. This is treated as the parameters of the «Gauss» beam spot in simulation of the flux by MCNPX. The shape of beam shown on the right panel in Fig.4 was used and sign as «real» beam in simulation.

3. MEASUREMENT PROCEDURE

The gamma-ray measurements have been performed using the HPGe detectors (see Table 3). All measurements have been carried out without any filters. First measurements of samples were started after 2.4 h from the stop of irradiation.

Table 3. Characteristics of the two HPGe detectors used for gamma-ray measurements

HPGe detector	CANBERRA GR1819	ORTEC (planar) GeLP 36360/13
Relative efficiency	18.9 %	Diam. 36 mm Thick. 13 mm
Resolution	1.78 keV (E_γ 1332 keV)	335 eV at 5.9 keV 580 eV at 122 keV

Measurement times were varied from 0.5 to 24 h. All measurements have been performed within 29 d. We find that only those residual nuclei can be studied which have half-life in the range of half an hour to one month. In Fig. 5 measurement time (shown as a pulse) and delayed time (shown as line) have been plotted for the CANBERRA (histograms marked as *A*) and X-ray detectors (histograms marked as *B*) for Th and U samples. CANBERRA detector is used to provide information of peaks ranging from 20 keV to 3 MeV and ORTEC detector is used for ~5 keV to 700 keV.

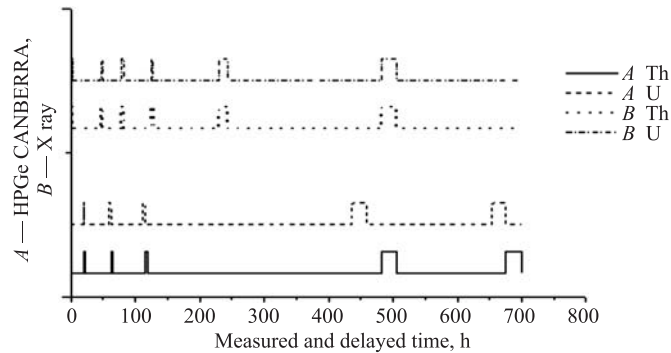


Fig. 5. Schedule of measurement of Th and U samples using two detectors

Processing of measured data of gamma rays was performed by interactive mode of the DEIMOS code [13]. Energy calibration, subtraction of background gamma-ray lines and single and double escape peaks, efficiency calibration and determination of experimental half-lives were made by a system of codes [14, 15]. Hundreds of gamma-ray lines are analyzed. Identification of nuclei was made when energy, half-life and intensity of peaks agree with the values in literature. A special attention to multiplex peaks has been emphasized.

4. METHOD OF ANALYSIS

From every i th spectrum we analyzed all observed gamma-ray peaks with energy $E_\gamma(j)$ and their area under the peak $S(j, i)$ measured with absolute efficiency $\varepsilon_\gamma^{\text{abs}}(j)$. Rate of production $Q(A_r, Z_r, i, j)$ of radioactive nucleus with decay constant λ , mass number A_r and atomic number Z_r , and intensity per decay $I_\gamma(j)$ can be determined from the following relation:

$$Q(A_r, Z_r, j, i) = \frac{S(j, i)\eta_A(Z_t, j)\eta_B(\lambda)\eta_C(j)\eta_D e^{\lambda t_2(i)} t_{\text{real}}(i)}{\varepsilon_\gamma^{\text{abs}}(j)I_\gamma(j)(1 - e^{-\lambda t_1})(1 - e^{-\lambda_{\text{real}}(i)}) t_{\text{live}}(i)}. \quad (1)$$

Here, t_1 , $t_2(i)$, $t_{\text{real}}(i)$ and $t_{\text{live}}(i)$ are the irradiation, cooling, real, and live measurement times. The coefficient $\eta_A(Z_t, j)$ accounts for the self-absorption of gamma-ray in the sample with Z_t . The $\eta_B(\lambda)$ is the correction for fluctuation of beam intensity and it is determined for each residual product nucleus. The $\eta_C(j)$ is the coincidence summing correction, and the η_D is the correction for nonpoint geometry of measured sample. More detailed explanation of all these corrections are given in Subsecs. 4.1–4.3.

The average value of $Q(A_r, Z_r, i)$ from i th spectrum was calculated as the weighted mean value $Q(A_r, Z_r, i, j)$ for different gamma transitions j ; and further the final $Q(A_r, Z_r)$ value was received in the same way from all i spectra. This procedure is applied to monitor samples and the results of the number of incident deuterons per second N_d [s^{-1}] are obtained from the following relation:

$$N_d = \frac{Q(A_r, Z_r)}{\sigma(A_r, Z_r) N_s}. \quad (2)$$

Here $\sigma(A_r, Z_r)$ is the reaction cross section [cm^2]. N_s is the number of atoms on the surface of the target [$\text{atom} \cdot \text{cm}^{-2}$] is given by the formula:

$$N_s = \frac{N_{\text{avo}} m}{AS}. \quad (3)$$

It assumes that all atoms along the thickness are subjected to the interaction with projectile. N_{avo} is Avogadro constant ($6.0221415 \cdot 10^{23}$ [mol^{-1}]), m is the mass

[g] and A is the mass number of target expressed in grams, S is the surface area of the target [cm^2], and N_t — number of atoms in the target ($N_t = SN_s$).

The $B(A_r, Z_r)$ value can be defined as number of produced residual nuclei with A_r, Z_r per one gram of sample and per one incident deuteron. The reaction rate $R(A_r, Z_r)$ is ratio of number of produced residual nuclei per number of atoms in the sample and per number of incident deuterons:

$$R(A_r, Z_r) = \frac{Q(A_r, Z_r)}{N_t N_d}. \quad (4)$$

From these definitions we can deduced the following relation: $R(A_r, Z_r) = B(A_r, Z_r) A_t / N_{\text{avo}}$. On the other hand, for the theoretical calculation of the reaction rate we have used the relation

$$R(A_r, Z_r) = \int_{E_{\text{thr}}(A_r, Z_r)}^{\infty} \sigma(A_r, Z_r, E_n) \Phi(E_n) dE_n. \quad (5)$$

Here, $\Phi(E_n)$ is the neutron fluency [$\text{neutrons} \cdot \text{cm}^{-2} \cdot \text{MeV}^{-1} \cdot \text{deuteron}^{-1}$] passing through the sample. E_{thr} is the threshold neutron energy for the given reaction. Calculated values of R are displayed in Figs. 10–14 and Table 9 for different reactions.

Transmutation power $P(A_r, Z_r)$ may be defined as the quantity of produced elemental mass $m(A_r, Z_r)$ per unit mass of the target $m(A_t, Z_t)$. It may be written as the transmutation rate:

$$P(A_r, Z_r) = \frac{m(A_r, Z_r)}{m(A_t, Z_t)}. \quad (6)$$

Mass in terms of number of atoms N may be given by

$$m(A_i, Z_i) = \frac{N(A_i, Z_i) A_i}{N_{\text{avo}}}, \quad (7)$$

where $i = r$ or t . Writing normalized activity $a(A_r, Z_r)$ as a function of all residual nuclei produced in irradiation whether they survive or not:

$$a(A_r, Z_r) = \lambda(A_r, Z_r) N(A_r, Z_r). \quad (8)$$

$N(A_r, Z_r)$ may be calculated from Eq. (7). Abanades et al. [4] have expressed transmutation power in terms of the normalized activity $a(A_r, Z_r)$ (without accounting for the decay of (A_r, Z_r) nuclei during the irradiation) as follows:

$$P(A_r, Z_r) = \frac{A_r \cdot a(A_r, Z_r)}{\lambda(A_r, Z_r) m(A_t, Z_t) N_{\text{avo}}}. \quad (9)$$

Alternatively, using Eq. (4) for reaction rate $R(A_r, Z_r)$ in terms of the production rate $Q(A_r, Z_r)$ and number of residual nuclei which were produced during irradiation time t_{irr} , whether they survive as such or not, can be known simply by multiplying $Q(A_r, Z_r)$ by t_{irr} :

$$N(A_r, Z_r) = Q(A_r, Z_r)t_{\text{irr}}. \quad (10)$$

Transmutation power of a system can be given in terms of the reaction rate and not of the normalized activity by

$$P(A_r, Z_r) = R(A_r, Z_r)N_d \frac{A_r}{A_t}. \quad (11)$$

Here $N_d t_{\text{irr}} = N_D$ (an integral number). With normalization to 10^9 beam particles (protons or deuterons, etc.) we have

$$P_{\text{norm}}(A_r, Z_r) = 10^9 \frac{P(A_r, Z_r)}{N_D}. \quad (12)$$

4.1. Self-Absorption Correction. The coefficient $\eta_A(Z_t, E(j))$, used in relation (1) accounts for the self-absorption of gamma ray in the sample (A_t, Z_t) of thickness d , has been calculated as follows:

$$\eta_A(Z_t, E(j)) = \frac{\mu(Z_t, E(j))d}{1 - e^{-\mu(Z_t, E(j))d}}, \quad (13)$$

where $\mu(Z_t, E(j))$ is the total attenuation coefficient for a given γ -ray with energy $E_\gamma(j)$ in the source material of the target. The values of attenuation coefficients

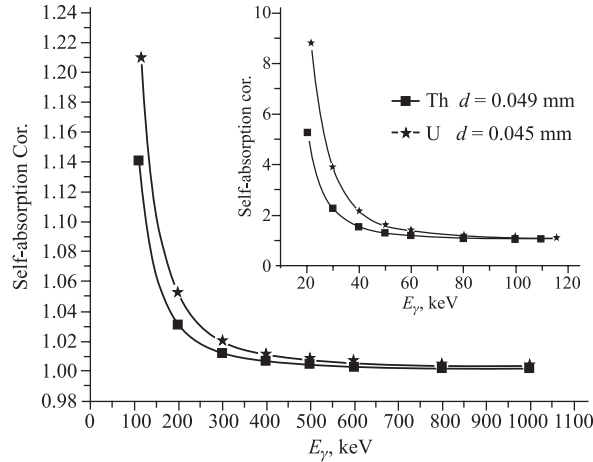


Fig. 6. Self-absorption correction η_A for Th and U samples as function of E_γ

for the two elements and different gamma energies are taken from [16], where precision in calculation are $\sim 2\%$. The corresponding η_A are shown as thick points in Fig. 6. The thin curves corresponds to $\eta_A = \{\exp[a_0 + a_1(\ln E) + a_2(\ln E)^2 \dots]\}^{-1}$ and this provides interpolation between the thick points for the required energy of the peak. This correction for the γ -ray of energy higher than 300 keV turned out to be less than 1.2% in the Th target and less than 2.2% in the U target. The dependence of $\eta_A(Z_t, E(j))$ on energy of γ -ray for Th and U targets is given in Fig. 6.

4.2. Correction for Beam Fluctuation. Similarly, $\eta_B(\lambda)$ the correction for fluctuation of beam intensity has been performed for each residual product with decay constant λ using the following relation:

$$\eta_B(\lambda) = \frac{1 - e^{-\lambda t_1}}{t_{\text{irr}} \sum_i^N \left\{ \frac{1}{t_p(i)} W(i) e^{-\lambda t_e(i)} (1 - e^{-\lambda t_p(i)}) \right\}}, \quad (14)$$

where t_{irr} is the total irradiation time and $t_p(i)$ is the start and $t_e(i)$ is the end time of the i th pulse. Fraction $W(i)$ is the number of deuterons in a single

Table 4. Corrections for ^{232}Th , $E_d = 1.60$ GeV

Isotope Energy, keV	Beam corr. η_B Self-abs. η_A	Sum coin. η_C CANBERRA	Sum coin. η_C X-ray	Full corr. = η_A $\eta_B \eta_C$ CANBERRA	Full corr. = η_A $\eta_B \eta_C$ X-ray
Th-231	$\eta_B = 0.992$				
25.646	$\eta_A = 3.030$	1.0053	1.0096	3.1651	3.1786
81.227	1.073	1.0351	1.0751	1.1018	1.1444
84.216	1.067	1.0043	1.0071	1.0630	1.0660
89.944	1.058	1.0187	1.0390	1.0692	1.0905
Pa-233	0.9997				
75.354	1.088	1.0481	1.0467	1.1400	1.1385
86.814	1.063	1.0476	1.0461	1.1133	1.1117
103.941	1.038	1.0475	1.0458	1.0870	1.0851
300.110	1.012	1.0034	1.0057	1.0151	1.0175
311.890	1.011	1.0063	1.0114	1.0171	1.0228
340.710	1.009	1.0023	1.0034	1.0110	1.0121
375.450	1.008	0.9717	0.9732	0.9792	0.9807
398.620	1.007	0.9167	0.9215	0.9228	0.9277
415.760	1.006	0.9625	0.9650	0.9680	0.9735
Mo-99	0.9969				
140.681	1.075	1.0050	1.0040	1.0770	1.0760
181.063	1.040	1.0680	1.0293	1.1073	1.0672
739.500	1.003	1.1149		1.1148	

i th pulse divided by the total number of deuterons. N is the total number of recorded pulses.

4.3. Coincidence Summing and Nonpoint Geometry Correction. Coincidence summing correction $\eta_C(j)$ has been calculated using the program COICOR.

Table 5. Corrections for ^{238}U , $E_d = 1.60$ GeV

Isotope Energy, keV	Beam corr. η_B Self-abs. η_A	Sum coin. η_C (CANBERRA)	Sum coin. η_C (X-ray)	Full corr. = η_A $\eta_B\eta_C$ (CANBERRA)	Full corr. = η_A $\eta_B\eta_C$ (X-ray)
Np-239	$\eta_B = 0.9964$				
106.125	$\eta_A = 1.084$	1.0276	1.0377	1.110	1.121
209.753	1.054	1.0401	1.0759	1.092	1.130
228.183	1.044	1.0097	1.0748	1.050	1.140
277.599	1.028	1.0384	1.0730	1.064	1.099
315.879	1.021	0.9218	0.9172	0.938	0.933
334.309	1.019	0.8302	0.8243	0.843	0.837
Mo-99	0.9969				
140.681	1.150	1.0050	1.0040	1.152	1.151
181.063	1.078	1.0680	1.0293	1.148	1.106
739.500	1.005	1.1149		1.117	
Te-132	0.9973				
49.720	1.591	1.096	1.130	1.739	1.793
228.160	1.044	1.017	1.026	1.059	1.068
522.650	1.008	1.279	1.161	1.286	1.167
630.190	1.006	1.153	1.095	1.157	1.099
667.72	1.006	1.162	1.092	1.123	1.055
772.61	1.005	1.135		1.096	
954.55	1.004	1.269		1.229	
I-133	0.9902				
529.87	1.008	1.0000	1.0000	0.998	0.998
I-135	0.9703				
546.557	1.008	1.0625		1.039	
1131.511	1.003	1.0578		1.029	
1260.409	1.003	1.0131		0.986	
1457.560	1.003	1.0000		0.973	
1678.027	1.003	0.9656		0.940	
1791.196	1.003	1.0000		0.973	
Xe-135	0.9753				
249.760	1.035	1.0006	1.0008	1.010	1.010
Ba-140	0.9993				
29.964	3.901	1.0269	1.0206	4.003	3.978
328.762	1.019	1.1999	1.0660	1.210	1.085
487.021	1.009	1.0989	1.0482	1.108	1.057
537.261	1.008	1.0135	1.0269	1.021	1.034
1596.210	1.003	1.1280		1.131	
Ce-143	0.9938				
57.356	1.380	1.0570	1.0561	1.450	1.448
293.266	1.025	1.0197	1.0302	1.039	1.049
664.571	1.006	1.0002	1.0167	1.000	1.017
721.929	1.005	0.9864		0.985	

More details of this program will be published shortly [17]. η_D is the correction for nonpoint geometry of the measured sample and for the distance of ~ 7 mm between the HPGe detector and the sample. This correction does not depend on energy of γ -ray and is less than 3 % for the radioactive source with diameter less than 15 mm. All accepted corrections are given for Th sample in Table 4 and for U sample in Table 5.

5. RESULTS OF MEASUREMENTS

Detailed results of measurements of γ -rays from ^{232}Th and $^{\text{nat}}\text{U}$ after irradiation by secondary neutrons generated from Pb target and uranium blanket during bombardment of 1.6 GeV deuteron beam are given in Tables 6 and 7. In these tables the data in the bold face correspond to the upper variable of the heading which is also shown in bold face. In the last column number of spectra is given

Table 6. Results of analysis of γ -ray spectra of ^{232}Th after irradiation by secondary neutrons from $E_d = 1.60$ GeV. All corrections are included. (+) denotes mixing due to other nuclide

Isotope	Activity, Bq	$T_{1/2}$ (Library)	$\langle B \rangle$	$\langle R \rangle$	Number of spectra
Energy, keV	I_g %	$T_{1/2}$ (Exper.)	B	R	
Th-231	56.3(56)	25.520(10) h	4.16(40)E-06	1.60(16)E-27	
25.646	14.50	27 h	3.96(51)E-06	1.53(20)E-27	2-X
81.227	0.89		1.87(45)E-05	7.1(17)E-27	1-X(+)
84.216	6.60	29 h	4.47(65)E-06	1.72(25)E-27	2-X
89.944	0.94	13(4) d	3.13(64)E-05	1.21(25)E-26	3-X(+)
Pa-233	42.1(14)	26.967(2) d	7.86(34)E-05	3.03(10)E-26	
75.354	1.39		5.4 (12)E-04	2.09(46)E-25	1-X(+)
86.814	1.97		7.5 (33)E-05	2.9(13)E-26	1-X
103.941	0.87	23(10) d	9.94(84)E-05	3.83(32)E-26	5-X
300.110	6.62	19(9) d	7.01(64)E-05	2.69(25)E-26	5-X
300.110	6.62	23(3) d	7.35(47)E-05	2.83(18)E-26	5-C
311.890	38.6	33.5(27) d	8.68(39)E-05	3.35(15)E-26	6-X
311.890	38.6	28.2(8) d	8.15(39)E-05	3.14(15)E-26	5-C
340.710	4.47	23(8) d	7.51(65)E-05	2.89(25)E-26	5-X
340.710	4.47	25(4) d	7.00(44)E-05	2.70(17)E-26	5-C
375.450	0.679	20(8) d	1.30(37)E-04	5.1(16)E-26	2-C
398.620	1.390	16(3) d	1.16(12)E-04	4.47(46)E-26	5-C(+)
415.760	1.745	17(3) d	7.36(71)E-05	2.84(27)E-26	5-C
Mo-99	1.04(12)	2.7475(4) d	1.98(23)E-07	7.63(89)E-29	
140.681	89.43	2.9(26) d	2.18(34)E-07	8.4(13)E-29	3-X
140.681	89.43	2.6(17) d	1.78(33)E-07	6.9(13)E-29	3-C

Table 7. Results of analysis of γ -ray spectra of ^{nat}U after irradiation with secondary neutrons from $E_d = 1.60$ GeV. All corrections are included. (+) denotes mixing due to other nuclide

Isotope Energy, keV	Activity, Bq I_g %	$T_{1/2}$ (Library) $T_{1/2}$ Exper.	$\langle B \rangle$ B	$\langle R \rangle$ R	Number of spectra
Np-239	849(40)	2.3565(4) d	7.51(35)-05	2.97(14)E-26	
106.125	27.2	2.388(15) d	6.76(30)E-05	2.67(12)E-26	6-X
106.125	27.2	2.39(6) d	6.51(40)E-05	2.64(16)E-26	3-C
209.753	3.42	2.36(5) d	9.54(43)E-05	3.77(17)E-26	5-X
209.753	3.42	2.44(10) d	9.00(52)E-05	3.56(21)E-26	3-C
228.183	10.76	2.45(6) d	8.86(37)E-05	3.50(15)E-26	6-X
228.183	10.76	2.49(4) d	8.51(54)E-05	3.36(21)E-26	3-C
277.599	14.38	2.35(3) d	7.37(33)E-05	2.91(13)E-26	5-X
277.599	14.38	2.45(9) d	7.47(53)E-05	2.96(21)E-26	3-C
315.879	1.60	1.8(3) d	7.70(63)E-05	3.04(25)E-26	4-X
315.879	1.60	2.30(12)d	7.12(64)E-05	2.81(25)E-26	2-C
334.309	2.07	2.04(14) d	6.25(52)E-05	2.47(21)E-26	5-X
334.309	2.07	3.2 d	5.15(51)E-05	2.03(20)E-26	2-C
Mo-99	14.1(16)	2.7475(4) d	1.45(17)E-06	5.74(65)E-28	
140.681	89.43	2.72(9) d	1.53(8)E-06	6.05(32)E-28	5-X
140.681	89.43	3.00(15) d	1.21(9)E-06	4.78(36)E-28	4-C
181.063	5.99	0.8 d	4.07(71)E-06	1.61(28)E-27	2-X
181.063	5.99		2.66(49)E-06	1.05(19)E-27	1-C
739.500	12.13	1.6 d	1.95(28)E-06	7.7(11)E-28	2-C
Te-132	11.5(10)	3.204(2) d	1.38(12)E-06	5.46(46)E-28	
49.720	15.0	4.7(11) d	2.03(20)E-06	8.3(8)E-28	6-X
49.720	15.0		5.8(17)E-06	2.3(7)E-27	1-C
228.160	88.0	2.45(6) d	7.86(39)E-06	3.11(15)E-27	6-X +
228.160	88.0	2.49(4) d	3.19(24)E-06	1.26(9)E-27	4-C +
522.650	16.6	8(4) d	1.47(23)E-06	5.7(9)E-28	3-C
630.190	13.3		0.98(28)E-06	3.9(11)E-28	1-C
667.72	101.7	2.47(29) d	1.38(9)E-06	5.5(4)E-28	3-C
772.61	77.9	3.4(5) d	1.23(9)E-06	4.9(4)E-28	3-C
954.55	18.7	4.0(21) d	1.33(17)E-06	5.2(7)E-28	3-C
I-133	35(18)	20.8(1) h	8.0(41)E-07	3.2(16)E-28	
529.87	86.3	14.4 h	1.28(405)E-06	5.1(7)E-28	2-X
529.87	86.3	20 h	4.51(343)E-07	1.78(22)E-28	2-C
I-135	175(14)	6.57(2) h	1.80(26)E-06	7.13(57)E-28	
546.557	7.20		2.04(48)E-06	8.0(19)E-28	1-C
1131.511	22.74		1.81(31)E-06	7.2(12)E-28	1-C

Table 7 (continuation)

1260.409	28.90		1.76(28)E-06	7.0(11)E-28	1-C
1457.560	8.73		1.34(37)E-06	5.3(15)E-28	1-C
1678.027	9.62		2.15(44)E-06	8.5(17)E-28	1-C
1791.196	7.77		1.88(38)E-06	7.5(15)E-28	1-C
Xe-135	152(58)	9.14(2) h	2.04(109)E-06	8.6(38)E-28	
249.760	89.9	16.6(33) h	1.21(59)E-06	5.80(235)E-28	3-X
249.760	89.9	10.7(10) h	3.44(81)E-06	1.37(32)E-27	2-C
Ba-140	3.38(10)	12.752(3) d	1.62(5)E-06	6.40(19)E-28	
29.964	14.1		3.0(13)E-06	1.4(5)E-27	1-X
328.762	20.3	30(40) d	2.5(14)E-06	6.4(30)E-28	3-C
487.021	45.5	18(11) d	1.57(15)E-06	6.20(59)E-28	3-C
537.261	24.39	17(5) d	2.3 (14)E-06	8.9(55)E-28	4-C
1596.210	95.4	11.5(20) d	1.62(5)E-06	6.41(20)E-28	5-C
Ce-143	24.5(54)	33.039(6) h	1.26(27)E-06	5.0(11)E-28	
57.356	11.7	32.4 h	2.19(25)E-06	8.7(10)E-28	2-X
57.356	11.7		1.61(48)E-06	6.3(19)E-28	1-C
293.266	42.8	33.6 h	1.54(20)E-06	6.0(8)E-28	2-X
293.266	42.8	103(36) h	7.1 (14)E-07	2.8(6)E-28	4-C
664.571	5.69	60 h	1.75(64)E-06	6.9(25)E-28	2-C

where γ -ray was observed and the letter X denotes the planar detector and letter C denotes coaxial detector.

We can see that there is good agreement between corresponding values measured by different detectors. The plus sign in brackets (+) shows that given γ -line is a doublet, i.e., the intensity is the sum of two γ -rays following beta decay of different isotopes.

6. SIMULATION OF NEUTRON FLUX

Monte Carlo code MCNPX v2.6.C was used to simulate the production and transport of secondary particles in the setup [18]. The particle production is handled by several spallation models, which describe the reaction in two steps: intranuclear cascade with preequilibrium stage (INC), and evaporation stage (EVAP). Two combinations of newer models (from several included in MCNPX) were used in simulations: CEM03 INC with CEM03 EVAP and INCL4 INC with ABLA EVAP models.

The «Energy plus Transmutation» setup was implemented in the code with the parameters given in Fig. 1. The beam parameters (displacement and profile) were determined from a set of SSNT and activation detectors, placed in front of the target. The data from these detectors were fitted by the Gaussian profile

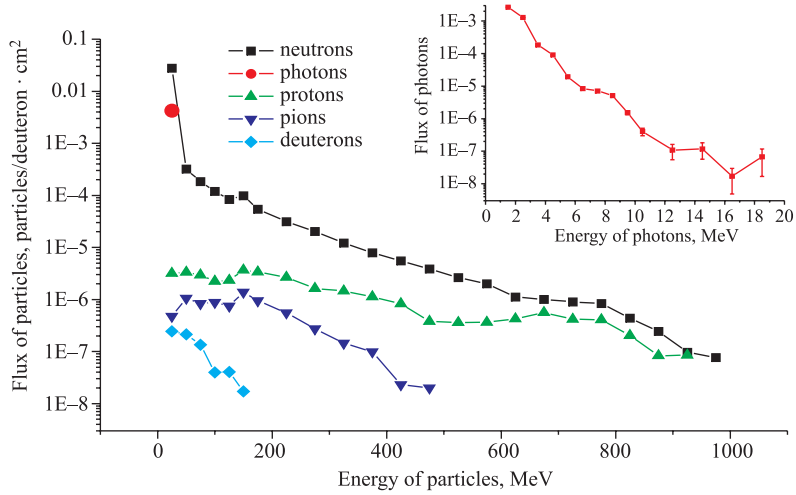


Fig. 7. The simulated neutron, photon, proton, pion and deuteron spectra on top of the second section of our setup using INCL model and real beam. Insert is spectrum of photon with energy from 0 to 20 MeV

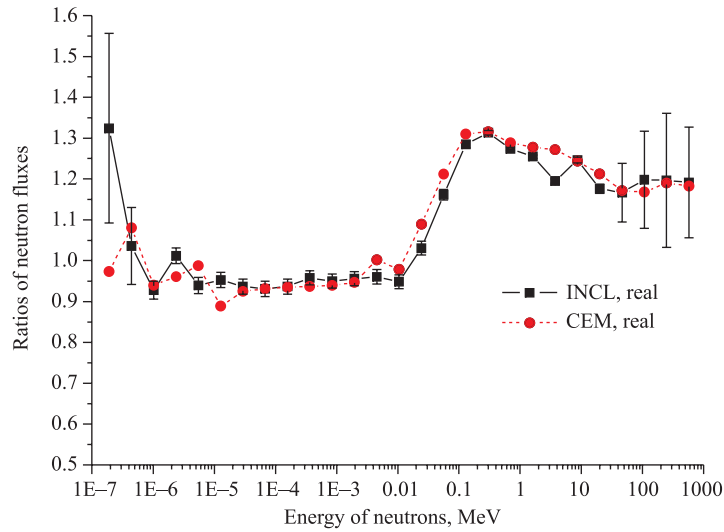


Fig. 8. Ratio of neutron flux in box 3 normalized to box 4. Two variants of simulation — «INCL + real beam» and «CEM + real beam» were performed

$x(\text{FWMH}) = 2.87 \text{ cm}$, $y(\text{FWMH}) = 1.92 \text{ cm}$, $x_c = -0.64 \text{ cm}$, $y_c = 0.39 \text{ cm}$ — in simulations referred with «Gauss», or the number of tracks from the SSNT

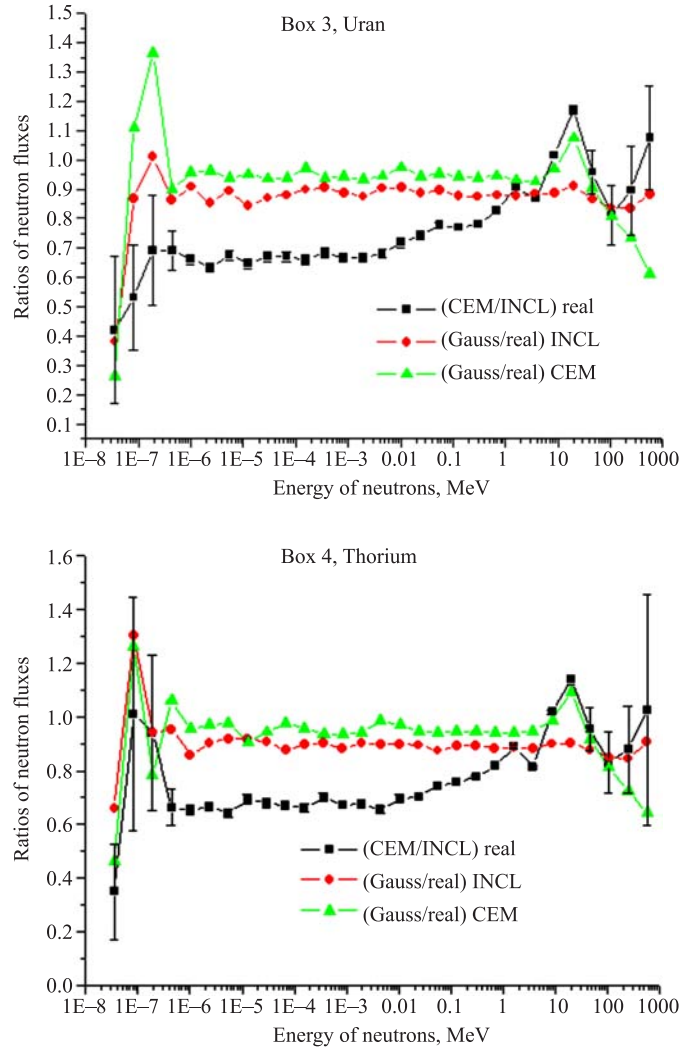


Fig. 9. Ratios of neutron flux simulated in box 3 (top panel) and box 4 (bottom panel) with different combinations of intranuclear model and shape of beam. $(\text{CEM/INCL})_{\text{real}}$ marks the ratio $\Phi(\text{CEM} + \text{real}) / \Phi(\text{INCL} + \text{real})$; $(\text{Gauss/real})_{\text{INCL}}$ corresponds to the ratio $\Phi(\text{INCL} + \text{Gauss}) / \Phi(\text{INCL} + \text{real})$; $(\text{Gauss/real})_{\text{CEM}}$ corresponds to the ratio $\Phi(\text{CEM} + \text{Gauss}) / \Phi(\text{CEM} + \text{real})$. The statistical uncertainty is shown only for one ratio $(\text{CEM/INCL})_{\text{real}}$ because for the next two ratios it is almost the same

detectors were directly used in the definition of the beam profile — in simulations referred with «real».

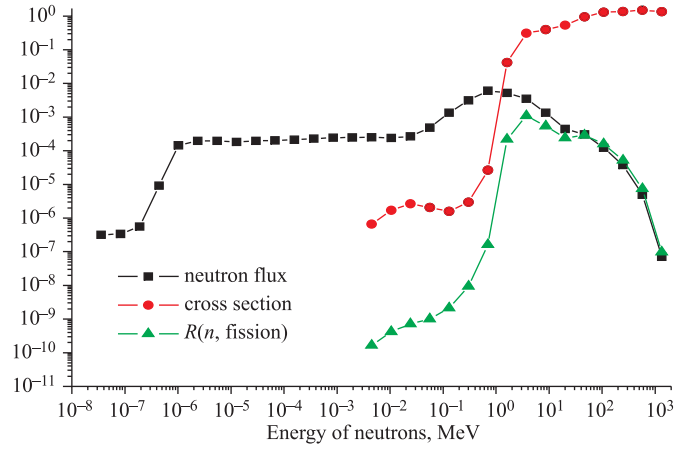


Fig. 10. Fission cross section, neutron flux and reaction rate of $^{232}\text{Th}(n, f)$, INCL, real beam

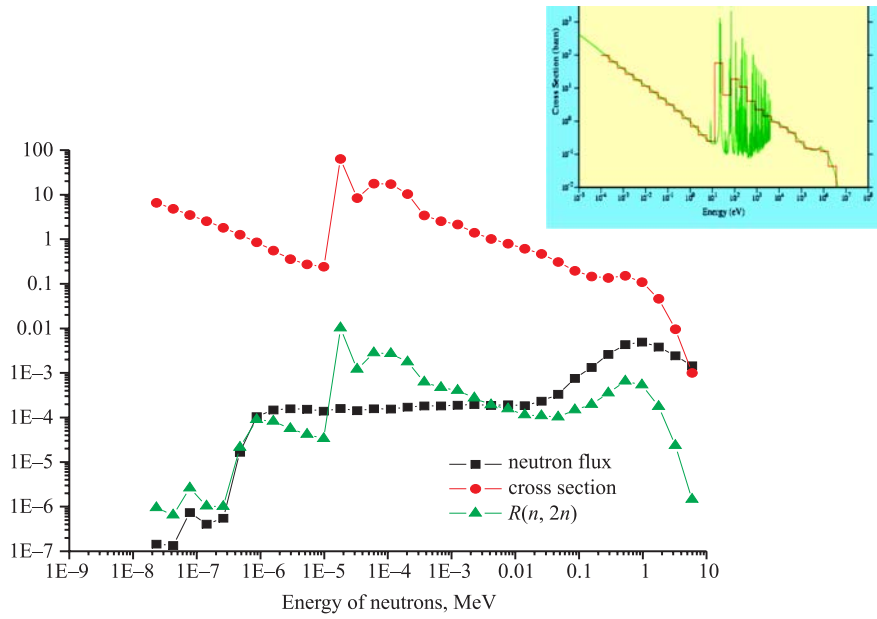


Fig. 11. Cross section, neutron flux and reaction rate of $^{232}\text{Th}(n, \gamma)$, INCL, real beam. Insert is pointwise (library JEFF-3.1) versus groupwise (code NJOY 99.112) cross section comparison

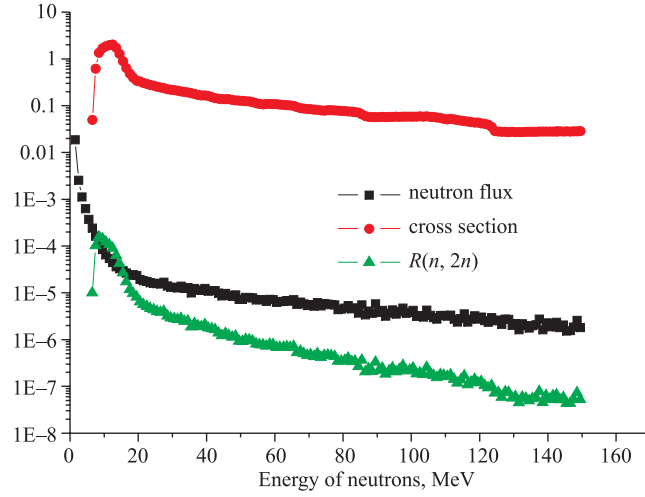


Fig. 12. Neutron flux, cross section and reaction rate of $^{232}\text{Th}(n, 2n)$, INCL, real beam

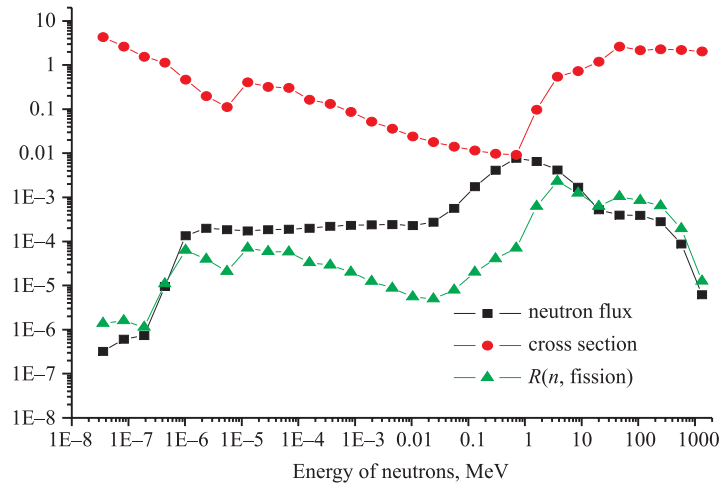


Fig. 13. Neutron flux, cross section and reaction rate of fission of ^{nat}U , INCL, real beam

The area of the setup above the second section containing the samples was divided into four boxes along the central line with dimensions of $36 \text{ mm} \times 36 \text{ mm} \times 1.5 \text{ mm}$ (see also caption of Fig. 2) and the fluxes of neutrons, protons, deuterons, pions, and photons [$\text{particles} \cdot \text{MeV}^{-1} \cdot \text{cm}^{-2}$] were calculated for each cell. The example of simulated spectra is shown in Fig. 7, with the total flux of neutrons $2.86 \cdot 10^{-2} \text{ n/cm}^2/\text{deuteron}$. The proton flux is 1000 times lower,

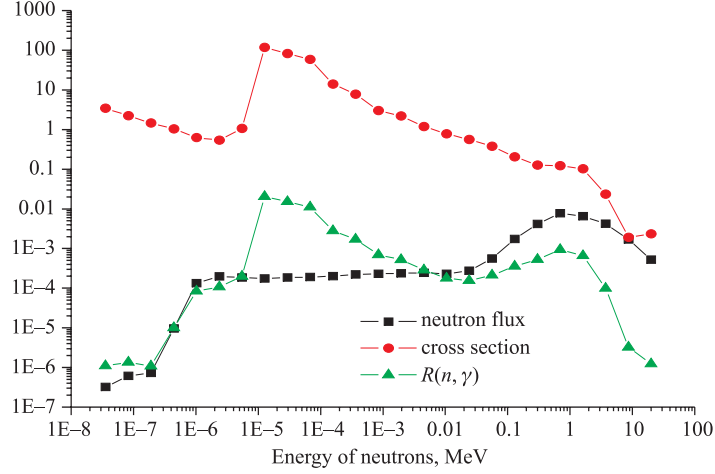


Fig. 14. Neutron flux, cross section and reaction rate of $^{nat}\text{U}(n, \gamma)$, INCL, real beam

and pion, deuteron, and photon fluxes are $2 \cdot 10^4$, $5 \cdot 10^5$, and 5 times lower than neutron flux, respectively. In Fig. 8 ratios of neutron fluxes in box 3 are normalized with respect to box 4 for two cases of simulation — «INCL + real beam» and «CEM + real beam» are given. No significant difference between these ratios outside the statistical uncertainties was observed. We can see that the ratio $\Phi(E_n(\text{box 3}))/\Phi(E_n(\text{box 4}))$ has wide maximum ~ 1.3 at $E_n > 0.2$ MeV. Small statistics has been used for the calculation of the points at the beginning and at the end of the spectrum. The neutron flux ratios calculated in box 3 (U – placed) and box 4 (Th – placed) for different combinations of intranuclear model and beam shape: «INCL + real», «INCL + Gauss», «CEM + real», «CEM + Gauss» are given in Fig. 9. The simulation by INCL model gives more neutrons with energy from 1 eV to 1 MeV (about from 30 to 20%) than simulation with CEM model. The shape of «real» beam simulates about 10 and 5% more neutrons ($E_n < 1$ MeV) for INCL and CEM than the «Gauss» shape of beam. It is seen that behavior ratios in box 3 and box 4 are very similar.

The reaction rate $R(A_r, Z_r)$, see Eq. (4), or $B(A_r, Z_r)$ value are calculated with the convolution of the simulated spectra of produced particles with the appropriate cross sections (F4+FM card in MCNPX), see Eq. (5). Up to 20 MeV, the cross sections which were used are included in the MCNPX code (from ENDF/B-VI library), missing cross sections for (n, γ) and (n, f) reactions in ^{235}U , ^{238}U and ^{232}Th were imported from JEFF-3.1 library [21]. Above 20 MeV, the spectra of produced particles were binned in 1 MeV bins (50 MeV bins above 150 MeV), and the number of particles in bins were multiplied with the

appropriate cross sections, calculated with the combination of the TALYS-1.0 code [22] and the MCNPX code using the CEM03 model [23].

Reaction rates of $^{232}\text{Th}(n, f)$, $^{232}\text{Th}(n, \gamma)$, $^{232}\text{Th}(n, 2n)$, $^{\text{nat}}\text{U}(n, f)$ and $^{\text{nat}}\text{U}(n, \gamma)$ are calculated by means of neutron flux estimated in box 3 (for U) and in box 4 (for Th) and also cross-section value given in the same way as was considered above. The dependences of neutron flux, cross sections and reaction rate on energy of neutrons are given for different reactions and samples in Figs. 10–14. Calculated reaction rates are established summing of partial ones $R(A_r, Z_r, E_n)$ from lowest until highest energy bin of neutrons. The results are given in Table 9. We evaluated using INCL model and real beam also $R(p, \text{fission})$ for ^{232}Th and $^{\text{nat}}\text{U}$ and received $3.57 \cdot 10^{-29}$ and $5.18 \cdot 10^{-29}$ which consist in 1.84 and 0.682% from the full amount of $R[(n, \text{fission}) + (p, \text{fission})]$. For $R(p, pn)$ reaction on ^{232}Th by means of the same variant of simulation we received $1.55 \cdot 10^{-30}$ which is 0.155% from full value of $R[(n, 2n) + (p, pn)]$.

7. RESULTS AND DISCUSSIONS

For evaluation of experimental value of fission reaction rate we made another distribution by condensing neutrons into two major groups in case of ^{238}U and ^{232}Th and three groups for ^{235}U because mass distribution of the fission products are available only for three various energies of neutrons, i.e., thermal (0.0252 eV) only for ^{235}U , unresolved resonance energy (400 keV) and high-energy neutrons (14 MeV). Thus, we divided neutrons into three major energy regions:

- thermal, epithermal and resonance — from $a(1) = 10^{-5}$ eV to $a(2) = 1.26 \cdot 10^5$ eV;
- unresolved resonance and fast neutrons — from $a(2) = 1.26 \cdot 10^5$ eV to $a(3) = 4.57 \cdot 10^6$ eV;
- fast and high energy neutrons — from $a(3) = 4.57 \cdot 10^6$ eV up to $a(4) =$ beam energy.

The weight factor of fission by neutron $w_j(t)$ with energy in region j is introduced as follows:

$$w_j(t) = \frac{\int_{a(j)}^{a(j+1)} \sigma_j(t, E_n) \Phi(E_n) dE_n}{\int_{a(1)}^{a(4)} \sigma_j(t, E_n) \Phi(E_n) dE_n}, \quad (15)$$

where $j = 1, 2, 3$ for ^{235}U and $j = 2, 3$ for ^{238}U and ^{232}Th , and t stands for different nuclei in the sample (for example, ^{235}U , ^{238}U and ^{232}Th of our samples). We performed manual integration of product of cross section and neutron flux into each region to obtain the weight factors (see Table 8). By means of these weights $w_j(t)$ and library of fission product yields $Y_{\text{cum}}(t, r, j)$ (JEFF-3.1) we

estimate mean weight yields, $Y_{\text{cum}}(t, r)$, where r stands for the observed fission product. For our experimental condition we have

$$Y_{\text{cum}}(\text{Th}, {}^{99}\text{Mo}) = w_2(\text{Th})Y_{\text{cum}}(\text{Th}, {}^{99}\text{Mo}, 2) + w_3(\text{Th})Y_{\text{cum}}(\text{Th}, {}^{99}\text{Mo}, 3), \quad (16)$$

$$Y_{\text{cum}}(\text{U}_{\text{nat}}, r) = [0.007204(w_1({}^{235}\text{U})Y_{\text{cum}}({}^{235}\text{U}, r, 1) + w_2({}^{235}\text{U})Y_{\text{cum}}({}^{235}\text{U}, r, 2) + w_3({}^{235}\text{U})Y_{\text{cum}}({}^{235}\text{U}, r, 3))] + [0.992742(w_2({}^{238}\text{U})Y_{\text{cum}}({}^{238}\text{U}, r, 2) + w_3({}^{238}\text{U})Y_{\text{cum}}({}^{238}\text{U}, r, 3))], \quad (17)$$

where $r = {}^{99}\text{Mo}$, ${}^{132}\text{Te}$, ${}^{133}\text{I}$, ${}^{135}\text{I}$, ${}^{135}\text{Xe}$, ${}^{140}\text{Ba}$, and ${}^{143}\text{Ce}$. In such approximation we can assume that the ratio between $R_{\text{exp}}(t, r)$ value for each observed fission product (r) and relative production yield $Y_{\text{cum}}(t, r)$ are constant for the same residual nucleus and for given sample ${}^{\text{nat}}\text{U}$ or ${}^{232}\text{Th}$ (see Fig. 15). If all

Table 8. Group weight factors for calculations of total number of fissions

Energy of secondary neutrons	${}^{232}\text{Th}$	${}^{235}\text{U}$	${}^{238}\text{U}$	${}^{\text{nat}}\text{U}$
Epithermal	$6.72 \cdot 10^{-7}$	0.636	$7.12 \cdot 10^{-5}$	$4.65 \cdot 10^{-3}$
Resonance	0.663	0.318	0.715	0.712
Fast	0.337	0.046	0.285	0.283

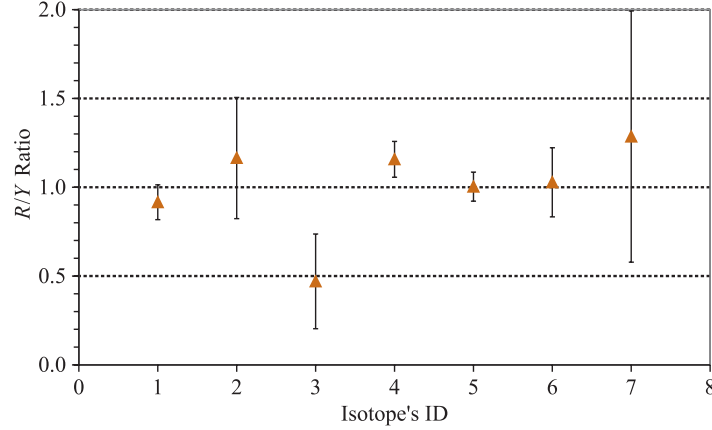


Fig. 15. The relative ratio of $R_{\text{exp}}({}^{\text{nat}}\text{U}, r) / (Y_{\text{cum}}({}^{\text{nat}}\text{U}, r))$ (here on X axis 1 — ${}^{99}\text{Mo}$, 2 — ${}^{132}\text{Te}$, 3 — ${}^{133}\text{I}$, 4 — ${}^{135}\text{I}$, 5 — ${}^{135}\text{Xe}$, 6 — ${}^{140}\text{Ba}$, and 7 — ${}^{143}\text{Ce}$)

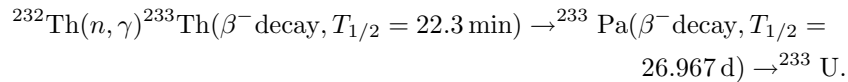
residual nuclei having different mass numbers, A_r are observed, it means that all decay chains of nuclei followed up to the observed residual nucleus, A_r are not partly covered up. Then we can pass from cumulative yield to corresponding sum of independent yields $\sum_r Y_{\text{ind}}(t, r)$ and from this, one can find total reaction rate for all residual nuclei. This gives the reaction rate of fission. Here, it is well known that the sum of independent yields is not identical with corresponding cumulative yield and the relation between them depends on the half-lives of nuclei in the decay chain [15]. If we identify several residual nuclei with the same mass number A_r , then we pass from cumulative yield to the sum of independent yields. Several independent yields appear two times, but we must accept only the last product nucleus. For example, we observed ^{135}I and ^{135}Xe from the $^{\text{nat}}\text{U}$ and we know that ^{135}I is accumulated from the decay chain $^{135}\text{Sn} \rightarrow ^{135}\text{Sb} \rightarrow ^{135}\text{Te} \rightarrow ^{135}\text{I}$ and similarly, ^{135}Xe is accumulated from $^{135}\text{Sn} \rightarrow ^{135}\text{Sb} \rightarrow ^{135}\text{Te} \rightarrow ^{135}\text{I} \rightarrow ^{135}\text{Xe}$. In this situation, we accept the sum of the independent yield for ^{135}Xe and not for ^{135}I . The experimental values $R_{\text{exp}}(n, \text{fission})$ for ^{232}Th and $^{\text{nat}}\text{U}$ targets calculated in such a method are given in Table 9.

Table 9. Comparison of the results of the experiment and calculation: INCL — intranuclear cascade, CEM — Cascade Exciton Model, real — the measured shape using the SSNTDs and Gaussian (the assumed shape of the beam with parameters given in Sec. 3)

Reaction	^{232}Th			$^{\text{nat}}\text{U}$	
	(n, γ)	(n, f)	$(n, 2n)$	(n, γ)	(n, f)
Reaction rate, exp.	3.03(10)E-26	5.89(60)E-27	1.60(16)E-27	2.97(14)E-26	2.24(10)E-26
R(CEM-Gauss)	1.46E-26	1.53E-27	1.18E-27	3.13E-26	6.32E-27
R(C-G>20MeV) [%]	0.004	52.4	25.9	0.006	32.9
R(CEM-real)	1.62E-26	1.76E-27	1.10E-27	3.26E-26	6.96E-27
R(C-r>20MeV) [%]		57.4			37.0
R(INCL-Gauss)	2.17E-26	1.71E-27	9.05E-28	4.49E-26	6.64E-27
R(I-G>20MeV) [%]		58.0			37.5
R(INCL-real)	2.49E-26	1.94E-27	9.98E-28	4.67E-26	7.59E-27
R(I-r>20MeV) [%]		58.2			38.4
R(C-G)/R(C-r)	0.90	0.87	1.07	0.96	0.91
R(C-G)/R(I-G)	0.67	0.89	1.30	0.70	0.95
R(C-r)/R(I-r)	0.65	0.91	1.10	0.70	0.92
R(I-G)/R(I-r)	0.87	0.88	0.91	0.96	0.87
R(exper.)/R(I-r,calc.)	1.22(4)	3.04(30)	1.60(15)	0.64(3)	2.95(13)
R(exper.)/R(C-r,calc.)	1.40(5)	3.35(33)	1.45(14)	0.91(4)	3.22(14)

Note: C-G sign CEM-Gauss, C-r _ CEM-real, I-G _ INCL-Gauss, I-r _ INCL-real.

The transmutation of ^{232}Th to ^{233}U proceeds mainly in the low energy neutron flux through the neutron capture reactions:



And the production rate of ^{233}Th is difficult to be estimated in our experiment firstly due its small half-life and secondly following its decay. There are only two gamma rays having intensity more than 1% per decay, i.e., 29.374 keV ($I_\gamma = 2.5\%$) and 86.477 keV ($I_\gamma = 2.7\%$). We did not observe these gamma rays, but we found nine gamma rays which correspond the beta decay of ^{233}Pa and allowed one to establish the reaction rate R with statistical error 3.3%. The distance d of the Th sample from the center of our setup is 13.1 cm.

We estimate the value of normalized transmutation power of ^{232}Th which is equal to $P_{\text{norm}}(^{233}\text{Pa}) = 3.09(13) \cdot 10^{-17} [\text{g} \cdot \text{g}^{-1}]$ for our setup. This can be compared with the following TARC data [4] which was obtained on irradiation of Pb target by protons. It may be mentioned that the secondary spallation neutrons were moderated in Pb assembly weighting ~ 334 t and its cross-sectional diameter, $d \sim 3.3$ m and length being 3 m. Comparison of some of the conditions of the two experiments with Th and $^{\text{nat}}\text{U}$ samples are given in Table 10. In the TARC experiment $P_{\text{norm}}(^{233}\text{Pa}) = 3.8(3) \cdot 10^{-17} [\text{g} \cdot \text{g}^{-1}]$ in hole 8 at $z = 22.5$ cm and at distance $x = 122$ cm and $P_{\text{norm}}(^{233}\text{Pa}) = 1.0(2) \cdot 10^{-17} [\text{g} \cdot \text{g}^{-1}]$ in hole 9 at $z = 7.5$ cm and at distance $x = 150$ cm (see Fig. 111 of [4]).

For the proposed ^{232}Th fuel the neutron multiplication from the $(n, 2n)$ nonfission reactions are not negligible. Furthermore, the chain of reactions is:

$$^{232}\text{Th} (n, 2n) ^{231}\text{Th} (\beta^- \text{ decay}, T_{1/2} = 25.52 \text{ h}) \rightarrow ^{231}\text{Pa} (\beta^- \text{ decay}, T_{1/2} = 32760 \text{ y}) \rightarrow ^{231}\text{U}(n, \gamma) \rightarrow ^{232}\text{U} (\alpha \text{ decay}, T_{1/2} = 68.9 \text{ y}).$$

It leads to the production of ^{232}U which is responsible for the large part of the short-term radiotoxicity, while ^{231}Pa is responsible for the long-term radiotoxicity. Data obtained from the planar HPGe detector are used for study of ^{231}Th . The most intensive gamma rays with energy 25.646 keV ($I_\gamma = 14.5\%$) and the 84.216 keV ($I_\gamma = 6.6\%$) were seen without any ambiguity.

In case of irradiation of Th sample we are able to identify only one fission product (^{99}Mo). Nevertheless, for this we evaluated the reaction rate for fission of ^{232}Th and it comes out to be $R_{\text{fission}}(^{232}\text{Th}) = 5.89(70) \cdot 10^{-27}$. From Eq. (16) weight yield of ^{99}Mo comes out to be $2.59(8) \cdot 10^{-2}$ per fission. The ratio of reaction rates, $R(n, 2n)/R(n, f)$ is about 27%.

Abanades et al. [4] measured $\text{Th}(n, 2n)$ reaction and placed Th samples at different distances from the center of TARC setup. Their experimental conditions are given in Table 10. They found for sample 1 placed at $d \sim 4$ cm, $B(^{231}\text{Th}) = 0.635(63) \cdot 10^{-6}$ and $1.32(13) \cdot 10^{-6}$ for $E_\gamma = 25.646$ and 84.216 keV, respectively. Similarly, for sample 2 placed at $d \sim 8.5$ cm $B(^{231}\text{Th}) = 1.05(16) \cdot 10^{-6}$ and $2.11(32) \cdot 10^{-6}$, for $E_\gamma = 25.646$ and 84.216 keV respectively. It can be revealed that TARC results for the two gamma energies are very different. From our experiment $B(^{231}\text{Th}) = 3.96(51) \cdot 10^{-6}$ for $E_\gamma = 25.646$ keV and $4.47(65) \cdot 10^{-6}$ for 84.216 keV, respectively, for the distance $d = 13.1$ cm from the centre of the «Energy plus Transmutation» setup. The two values are comparable with each other (see column 4 of Table 6).

Table 10. Comparison of some experimental conditions in TARC [4] irradiated with protons of momentum 3.5 and 2.75 GeV/c and our experiment with deuteron beam of 1.6 GeV energy

	²³² Th foils			^{nat} U foils	
	Our exp.	TARC		Our exp.	TARC
Reactions	(n, γ), (n, 2n)	(n, γ)	(n, 2n)	(n, γ)	(n, γ)
Weight (No.1), mg	93.2	132	158	172	290
Weight (No.2), mg			678		
Diameter (No.1), mm	15	12.7	12.5	15	12.7
Square (No.2), mm			30×29		
Thickness (No.1), μm	45.0	88.9	110.3	52.0	127
Thickness (No.2), μm			66.5		
Activity (No.1), Bq	378	536	624	2244	3783
Activity (No.2), Bq			2753		
Radial distance (No.1) Center – sample, mm	131	1220	~ 40	138	1070
Radial distance (No.2) Center – sample, mm		1500	~ 85		940
Beam particle	Deuteron	Proton	Proton	Deuteron	Proton
Beam energy	1.6 GeV	3.5 GeV/c	2. 5 GeV/c	1.6 GeV	3.5 GeV/c
Sum of particles	1.93.10 ¹³	2.14.10 ¹³		1.93.10 ¹³	2.14.10 ¹³
Sum of particle (No.1)			4.80.10 ¹²		
Sum of particle (No.2)			9.01.10 ¹²		
Irradiation time, h	6.65	8.5		6.65	8.5

The measured transmutation power estimated for (n, γ) reaction for ²³⁸U in our experiment is $P_{\text{norm}}(^{239}\text{U}) = 2.87(9) \cdot 10^{-17} [\text{g} \cdot \text{g}^{-1}]$, which again can be compared with TARC data $P_{\text{norm}}(^{239}\text{U}) = 1.1(3) \cdot 10^{-17} [\text{g} \cdot \text{g}^{-1}]$, and $7.7(2) \cdot 10^{-17} [\text{g} \cdot \text{g}^{-1}]$ for $z = -22.5$ cm and the hole 6 and hole 7 at $d = 107$ and 94 cm, respectively (see also Fig. 112 of Ref. [4]).

SUMMARY

The gamma-ray decays of the residual nuclei created in irradiation of Th and U samples by secondary neutrons were gathered into 32 spectra including the spectra of Al monitors. We observed and analyzed 157 peaks for which the energy, intensity and half-live were established and by means of these values the identification of the residual nuclei was done. Experimental reaction rates of ²³³Pa, ²³¹Th and ⁹⁹Mo in the ²³²Th sample and ²³⁹Np, ⁹⁹Mo, ¹³²Te, ¹³³I, ¹³⁵I,

^{135}Xe , ^{140}Ba , and ^{143}Ce in the U sample were evaluated. Comparing the reaction rates and relative yields for the fission products the experimental fission reaction rates of Th and U were determined.

Calculations of reaction rates for (n, γ) and $(n, \text{fission})$ on ^{232}Th , ^{235}U , and ^{238}U together with $(n, 2n)$ reaction on ^{232}Th were done. Two models — CEM (Cascade Exciton Model) and INCL (Intra-Nuclear Cascade Liege) and also two versions of the shape of the deuteron beam (the real and the Gaussian ones) were applied to the calculations, see Table 9. Ratios of the reaction rates from the experiment and the calculations for fissions of Th and U are about three when for the calculation of the CEM or INCL models and the real shape of the deuteron beam are employed. The (n, γ) reactions in Th and U are described by these models much better — deviations from experimental values do not exceed 40%. For $(n, 2n)$ reaction the experimental values are larger by about 45 and 60% than those calculated within the INCL and CEM models (Table 9). The calculations with the real and Gaussian shapes of the deuteron beam yield differences from 4 to 13% in both models. Ratios of the calculated reaction rates within the CEM and INCL models and with the real shape of the beam vary from 0.65 to 1.10.

At the end, it may also be mentioned that in our experiment calculated results suffer from the fact that there is no data library of neutrons with energy $E > 20$ MeV whether it is (n, γ) , (n, f) or $(n, 2n)$ reaction. In this situation, our cross sections at $E > 20$ MeV are estimated by TALYS and CEM03 codes. The influence of neutrons with energy > 20 MeV on the reaction rates $R(n, f)$ and $R(n, 2n)$ are shown in Table 9.

The evaluation of experimental fission reaction rate from reaction rate of different fission products is not very precise because we found only a few of them in case for uranium and only one for thorium sample. The yield of fission products are known with good accuracy only for three energy of neutrons. From these reasons the experimental values $R_{\text{exp}}(n, \text{fission})$ for ^{232}Th and $^{\text{nat}}\text{U}$ targets could have big enough systematic errors which were not included in the presented values.

Similarly, one can assume that on the low energy side of neutron spectrum there is uncertainty in estimation of the flux by a code. We know from our simulated flux by MCNPX that at $E_n = 0.87$ eV flux is small $\sim 1\%$ of the peak value and, for example, on assuming that if such flux exists up to thermal energy (0.025 eV) then the calculated reaction rates of $\text{Th}(n, \gamma)$ and $\text{U}(n, \gamma)$ will be enhanced by 82 and 18.6%, respectively, and as second assumption if the flux is zero in this region then these reaction rates will be decreased by 0.5 and 0.12%.

Second valid reason of these differences may be estimation of neutron flux taken from the Monte Carlo code (see Fig.9) which cannot be fully validated. These shortcomings can only be overcome in future and presently in the analysis of data of this experiment all other corrections are implemented in the best possible way.

The normalized transmutation power of (n, γ) and $(n, 2n)$ reactions on ^{232}Th and the (n, γ) reaction on ^{235}U were evaluated and compared with the data from TARC experiment (Table 10). For (n, γ) reactions our values P_{norm} for samples placed approximately 13 cm from the center of the «Energy plus Transmutation» setup are comparable with the TARC samples placed ~ 100 cm from the center of their setup. This can be explained from differences in neutron spectra (much more low-energy neutrons in TARC) and also from the fact that $\sim 70\%$ created neutrons do not escape their massive Pb target. The initiated proton energy at CERN was more than two times higher than our deuteron energy. The normalized transmutation power of the $(n, 2n)$ reaction on ^{232}Th is almost the same for our sample and the TARC samples placed at 4 and 8.5 cm from the center of the setup.

Acknowledgements. The authors are grateful to the operating crew of the Nuclotron accelerator of LHE, JINR Dubna for irradiation and good beam parameters, and Dr. Vera Bradnova for the experiment's minutes managing and photographic support. The authors are also grateful to METACentrum (Czech Republic) for offering computers for the calculations. The experiments were supported by the Czech Committee for the collaboration with JINR Dubna. Part of this work has been supported by grant of BRNS (DAE-India) and particularly by other grants and variable funding.

REFERENCES

1. *Janssen A.J.* Transmutation of Fission Products in Reactors and Accelerator-Driven Systems. ECN-R-94-001, January, 2004.
2. *Bhatnagar V.P., Casalta S., Hugon M.* Nuclear Waste Partitioning and Transmutation in the EURATOM Fifth and Sixth Framework. Talk presented at Seventh Information Exchange Meeting on Actinides and Fission Product Partitioning and Transmutation, Oct. 14–16, 2002, Jeju, Korea.
3. *Nifenecker H., Meplan O., David S.* Accelerator Driven Sub-Critical Reactors. Bristol and Philadelphia: Institute of Physics Publishing, 2003.
4. *Abanades A., Aleixandre J., Andriamonje S. et al.* // Nucl. Instr. Meth. A. 2002. V. 478. P. 577–730.
5. *Krivopustov M.I., Chultem D., Adam J. et al.* // Kerntechnik. 2003. V. 68. P. 48–55; *Krivopustov M.I., Pavliouk A.V., Malakhov A.I. et al.* JINR Preprint E1-2007-7. Dubna, 2007.
6. *Wan J.-S., Ochs M., Vater P. et al.* // Nucl. Instr. Meth. B. 1999. V. 155. P. 110–115.
7. *Banaigs J., Berger J., Dulfo J., Goldzahl L. et al.* // Nucl. Instr. Meth. 1971. V. 95. P. 307–311.

8. *Kozma P., Yanovsky V. V. // Czech. J. Phys. 1990. V. 40. P. 393.*
9. *Blocki J., Randrup J., Swiatecki W. J., Tsang C.F. // Ann. Phys. (NY). 1977. V. 105. P. 427.*
10. *Westmeier W. Private communication.*
11. *Morgan G. L., Alrick K. R., Saunders A., Cverna F. C. et al. // Nucl. Instr. Meth. B. 2003. V. 211. P. 297–304.*
12. *Zhuk I. V. Private communication.*
13. *Frana J. // J. Radioanal. Nucl. Chem. 2003. V. 257. P. 583–589.*
14. *Adam J., Pronskikh V. S., Balabekyan A. et al. JINR Preprint P10-2000-28. Dubna, 2000.*
15. *Adam J., Balabekyan A., Pronskikh V. S. et al. // Appl. Rad. Isot. 2002. V. 56. P. 607–613.*
16. *Storm E., Israel H. // Nuclear Data Tables A. 1970. V. 7. P. 563;*
Veigele W. J. // Atomic Data Tables. 1973. V. 5, No. 1. P. 51–111;
Hubbell J. H. // Int. J. Appl. Rad. Isot. 1982. V. 33. P. 1269.
17. *Adam J., Katovský K., Majerle M. (to be published).*
18. *Hendricks J. S. et al. MCNPX, version 2.6.c, LA-UR-06-7991, 2006.*
19. *Cugnon J. Cascade Models and Particle Production: A Comparison. Particle Production in Highly Excited Matter. ISBN 0-306-44413-5// NATO Science Series. B. 1993. V. 303. P. 271–293.*
20. *Zhuk I. V. et al. JINR Preprint P1-2002-184. Dubna, 2002.*
21. *Experimental Nuclear Reaction Data (EXFOR). IAEA-NDS, 2008.*
22. *Koning A. J. et al. // Proc. of the Intern. Conf. on Nuclear Data for Science and Technology, Santa Fe, USA, Sept. 26 – Oct. 1, 2004.*
23. *Mashnik S. G. et al. // J. Phys. Conf. Ser. 2006. V. 41. P. 340–351.*

Received on August 12, 2008.

Корректор *Т. Е. Попеко*

Подписано в печать 7.11.2008.

Формат 60 × 90/16. Бумага офсетная. Печать офсетная.

Усл. печ. л. 1,93. Уч.-изд. л. 2,72. Тираж 285 экз. Заказ № 56385.

Издательский отдел Объединенного института ядерных исследований
141980, г. Дубна, Московская обл., ул. Жолио-Кюри, 6.

E-mail: publish@jinr.ru

www.jinr.ru/publish/